Mutations in *IRF6* cause Van der Woude and popliteal pterygium syndromes

Shinji Kondo[1*], Brian C. Schutte[1,2*], Rebecca J. Richardson[3†], Bryan C. Bjork[4†], Alexandra S. Knight[3], Yoriko Watanabe[1], Emma Howard[3], Renata L.L. Ferreira de Lima[5], Sandra Daack-Hirsch[1], Achim Sander[6‡], Donna M. McDonald-McGinn[7], Elaine H. Zackai[7], Edward J. Lammer[8], Arthur S. Aylsworth[9], Holly H. Ardinger[10], Andrew C. Lidral[11], Barbara R. Pober[12], Lina Moreno[13], Mauricio Arcos-Burgos[14], Consuelo Valencia[14], Claude Houdayer[15], Michel Bahuau[15,16], Danilo Moretti-Ferreira[5], Antonio Richieri-Costa[17], Michael J. Dixon[3] & Jeffrey C. Murray[1,2,18]

*These two authors contributed equally to this work.

†These two authors contributed equally to this work.

‡Deceased.

Published online: 3 September 2002, doi:10.1038/ng985

Interferon regulatory factor 6 (IRF6) belongs to a family of nine transcription factors that share a highly conserved helix–turn–helix DNA-binding domain and a less conserved protein-binding domain. Most IRFs regulate the expression of interferon-α and -β after viral infection[1], but the function of IRF6 is unknown. The gene encoding IRF6 is located in the critical region for the Van der Woude syndrome (VWS; OMIM 119300) locus at chromosome 1q32–q41 (refs 2,3). The disorder is an autosomal dominant form of cleft lip and palate with lip pits[4], and is the most common syndromic form of cleft lip or palate. Popliteal pterygium syndrome (PPS; OMIM 119500) is a disorder with a similar orofacial phenotype that also includes skin and genital anomalies[5]. Phenotypic overlap[6] and linkage data[7] suggest that these two disorders are allelic. We found a nonsense mutation in *IRF6* in the affected twin of a pair of monozygotic twins who were discordant for VWS. Subsequently, we identified mutations in *IRF6* in 45 additional unrelated families affected with VWS and distinct mutations in 13 families affected with PPS. Expression analyses showed high levels of *Irf6* mRNA along the medial edge of the fusing palate, tooth buds, hair follicles, genitalia and skin. Our observations demonstrate that haploinsufficiency of *IRF6* disrupts orofacial development and are consistent with dominant-negative mutations disturbing development of the skin and genitalia.

To identify the locus associated with VWS, we carried out direct sequence analysis of genes and presumptive transcripts in the 350-kilobase (kb) critical region[3]. This approach is confounded by single-nucleotide polymorphisms (SNPs), normal DNA sequence variation that occurs about once every 1,900 base pairs[8] (bp). To distinguish between putative disease-causing mutations and SNPs, we studied a pair of monozygotic twins discordant for the VWS phenotype and whose parents were unaffected. Monozygotic status was confirmed by showing complete concordance of genotype at 20 microsatellite loci. We proposed that the only sequence difference between the twins would result from a somatic mutation found only in the affected twin. We identified a nonsense mutation in exon 4 of *IRF6* in the affected twin, which was absent in both parents and the unaffected twin (Fig. 1*a*). We subsequently identified mutations in 45 additional unrelated families affected with VWS and in 13 families affected with PPS (Fig. 1*b*; Table 1), demonstrating unequivocally that these two syndromes are allelic[6,7]. These mutations were not observed in a minimum of 180 control chromosomes.

Clefts of the lip with or without cleft palate and isolated cleft palate are developmentally and genetically distinct[9], yet VWS is a single-gene disorder that encompasses both clefting phenotypes. To verify this, we analyzed pedigrees ($n = 22$) that had a single mutation in *IRF6* and affected individuals with both phenotypes. Genotype analysis of family VWS25 demonstrated that affected individuals, regardless of their phenotype, shared the 18-bp deletion found in the proband (Fig. 1*a*). We observed similar results in the other families and conclude that a single mutation in *IRF6* can cause both types of cleft.

[1]*Department of Pediatrics and* [2]*Interdisciplinary PhD Program in Genetics, The University of Iowa, Iowa City, Iowa 52242, USA.* [3]*School of Biological Sciences and Department of Dental Medicine and Surgery, University of Manchester, Oxford Road, Manchester, UK.* [4]*Harvard University, Brigham and Women's Hospital, Boston, Massachusetts, USA.* [5]*Servico de Aconselhamento, Genetico da Universidade Estadual Paulista, Botucatu S.P., Brazil.* [6]*Clinic of Oral-Maxillofacial Surgery, University of Hamburg, Hamburg, Germany.* [7]*Division of Human Genetics and Molecular Biology, The Children's Hospital of Philadelphia, Philadelphia, Pennsylvania, USA.* [8]*Medical Genetics, Children's Hospital, Oakland, California, USA.* [9]*Department of Pediatrics and Genetics, University of North Carolina, Chapel Hill, North Carolina, USA.* [10]*Department of Pediatrics, University of Kansas, Children's Medical Center, Kansas City, Kansas, USA.* [11]*Department of Orthodontics, The University of Iowa, Iowa City, Iowa, USA.* [12]*Department of Genetics, Yale University School of Medicine, New Haven, Connecticut, USA.* [13]*PhD Program in Oral Sciences, The University of Iowa, Iowa City, Iowa, USA.* [14]*Universidad de Antioquia, Medellin, Colombia.* [15]*Service de Biochimie et Biologie Moléculaire, Hôpital d'Enfants Armand-Trousseau, Paris, France.* [16]*Service de Chirurgie Maxillofaciale et Plastique, Stomatologie, Hôpital d'Enfants Armand-Trousseau, Paris, France.* [17]*Departmento de Genetica Clinica, Hospital de Pesquisa e Reabilitacao de Lesoes Labio-Palatais, Universidade de São Paulo, Bauru, Brazil.* [18]*Department of Biology, The University of Iowa, Iowa City, Iowa 52242, USA. Correspondence should be addressed to J.C.M. (e-mail: jeff-murray@uiowa.edu).*

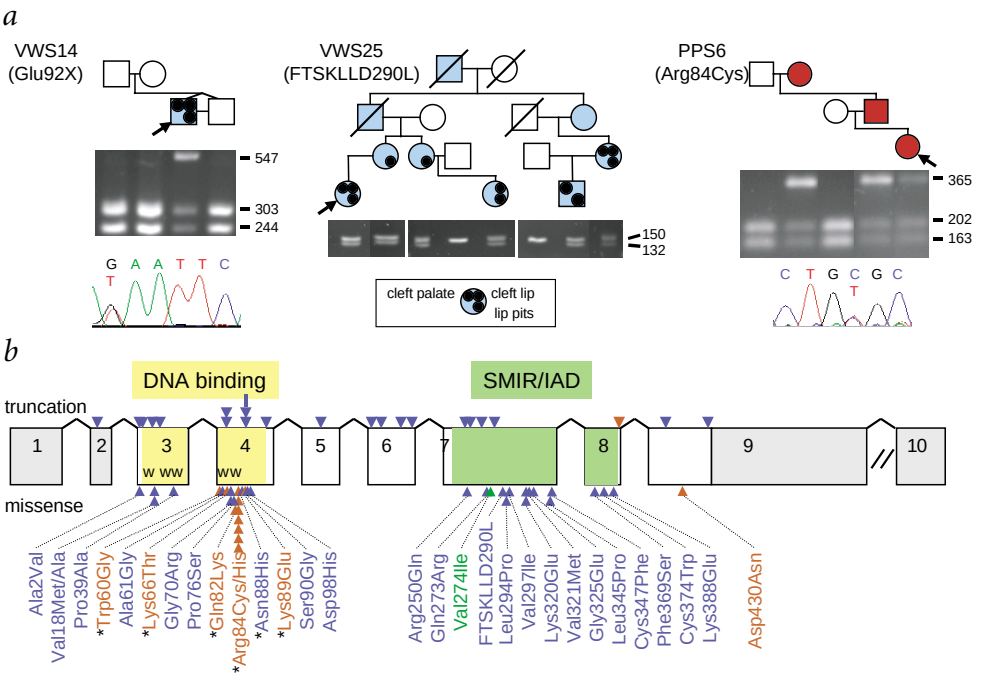

Fig. 1 Mutations in *IRF6* cause VWS and PPS. ***a***, Family number and mutation found for two VWS pedigrees and one PPS pedigree. The gender of each individual was randomly assigned to preserve the anonymity of the pedigrees; the actual pedigrees are available on request. Unaffected individuals (open), probands (arrow) and individuals with VWS (blue) or PPS (red) are indicated. Symbols representing specific phenotypes are shown below the pedigree for family VWS25. The sequence chromatogram derived from the affected proband is shown below the pedigrees for families VWS14 and PPS6. Above is an image of an agarose gel that shows the restriction-fragment length polymorphism (RFLP) assay used to confirm these mutations. Numbers on the side of each gel represent the size of the RFLP products. The mutation in family VWS14 abolishes an *Eco*RI restriction site, whereas the mutation in family PPS6 abolishes an *Hha*I site. Consequently, individuals with either mutation exhibit the large undigested DNA fragment in addition to two smaller digested products. Below the pedigree for VWS25 is an image of an agarose gel used to detect the 18-bp deletion mutation (132-bp fragment) or the wildtype allele (150-bp fragment). ***b***, The structure of the *IRF6* gene. Exons (rectangles) are drawn to scale except for exon 9, which is longer than shown. The brackets connecting the exons represent spliced introns, and the break between exons 9 and 10 represents an unspliced intron of 1,621 nt that is present in the most common 4.4-kb *IRF6* transcript. The untranslated portions are in gray. The predicted IRF6 protein contains a winged-helix DNA-binding domain (yellow) and a SMIR/IAD protein-binding domain (green). The DNA-binding domain includes a pentatryptophan (w) motif. The arrowheads indicate the relative position of protein-truncation (above exons) and missense mutations (below exons) that cause VWS (blue) or PPS (red) or that are polymorphisms (green). The arrow above exon 4 represents the Glu92X nonsense mutation identified in the affected twin of family VWS14. The amino-acid change for each missense mutation is shown and an asterisk indicates mutations affecting residues that contact the DNA.

To determine the effect of mutations on *IRF6* gene activity, we compared the type and position of the mutation with the phenotype. Previous identification of deletions encompassing the VWS locus (including *IRF6* in its entirety) had suggested that the phenotype is caused by haploinsufficiency[10–12]. In this study, we found protein-truncation (nonsense and frameshift) mutations in 22 families (Fig. 1*b*). Protein-truncation mutations were significantly more common in VWS than in PPS ($P = 0.004$) and were consistent with haploinsufficiency in the VWS pedigrees. The lone exception to this relationship was a nonsense mutation introducing a stop codon in place of a glutamine codon at position 393, found in pedigree PPS11, which may be a dominant-negative mutation (see below).

The position of the missense mutations provides insight into the structure and function of the *IRF6* gene product. When we aligned the family of IRF proteins, we observed that IRF6 has two conserved domains (Fig. 1*b*), a winged-helix DNA-binding domain (amino acids 13–113) and a protein-binding domain (amino acids 226–394) termed SMIR (Smad-interferon regulatory factor–binding domain)[13]. Studies of IRF3 and IRF7 have shown that the SMIR domain is required to form homo- and heterodimers[14,15]. The dimers then translocate to the nucleus, associate with other transcription factors and ultimately bind to their DNA targets[14]. Of the missense mutations, 35 of 37 localized to regions encoding these two domains. This distribution is non-random ($P < 0.001$), and we conclude that the domains are critical for IRF6 function.

Whereas the missense mutations that cause VWS were almost evenly divided between the two domains, most missense mutations that cause PPS were found in the DNA-binding domain (11 of 13, Fig. 1*b*). This distribution is significant ($P = 0.03$) and suggests that missense mutations in the DNA-binding domain associated with VWS and PPS affect IRF6 function differently. When we compared their positions with the crystal structure of the IRF1 DNA-binding domain[16], we found that every amino-acid residue that was mutant in individuals with PPS directly contacts the DNA, whereas only one of seven of the residues mutant in the individuals with VWS contacts the DNA. Most notably, we observed missense mutations involving the same residue, Arg84, in seven unrelated PPS families (Fig. 1*a*,*b*). The Arg84 residue is comparable to the Arg82 residue of IRF1. It is one of four residues that make critical contacts with the core sequence, GAAA, and is essential for DNA binding[16]. The observed change of this residue to a cysteine or histidine caused a complete loss of that essential contact (Fig. 2). One possible explanation for this apparent genotype–phenotype relationship is that missense mutations that cause VWS are due to a complete loss of function of the mutated IRF6 protein, affecting both DNA and protein binding, whereas missense mutations causing PPS affect only IRF6's ability to bind DNA. The ability of the mutated IRF6 to bind to other proteins is unaffected, and it therefore forms inactive transcription complexes; thus, this is a dominant-negative mutation. Similarly, deletion of the DNA-binding domain of IRF3 or IRF7 exerts a dominant-negative effect on the virus-induced expression of the type I interferon genes and the RANTES gene[15,17].

To correlate the expression of *IRF6* with the phenotypes of VWS and PPS, we carried out RT–PCR, northern-blot analysis and whole-mount *in situ* hybridization. We found that *Irf6* was broadly expressed in embryonic and adult mouse tissues (Fig. 3*a*,*b*), a pattern also seen in human fetal and adult tissues (data

not shown). Greater expression of *Irf6* seemed to occur in secondary palates dissected from day 14.5–15 mouse embryos and in adult skin. Whole-mount *in situ* hybridization demonstrated that *Irf6* transcripts were highly expressed in the medial edges of the paired palatal shelves immediately before, and during, their fusion (Fig. 3*d*). Similarly high *Irf6* expression was seen in the hair follicles and palatal rugae (Fig. 3*d*), tooth germs and thyroglossal duct (Fig. 3*f*) and external genitalia (Fig. 3*h*), and in skin throughout the body (data not shown). These observations are in accord with the VWS/PPS phenotype: notably, 20% of individuals with VWS exhibit agenesis of the second premolar teeth and 40% of individuals with PPS display genital anomalies.

Although we demonstrated that VWS and PPS are caused by mutations in a single gene, the phenotype for any given mutation varied in at least three ways even within the same family. Of the families with known mutations, we observed 32 families with multiple combinations of orofacial anomalies, 22 families with mixed clefting phenotypes (individuals with cleft lip and individuals with cleft palate only in the same family) and four families affected with PPS that included individuals who exhibit orofacial (VWS) features exclusively. The marked phenotypic variation in our cohort strongly implicates the action of stochastic factors or modifier genes on IRF6 function. In this context, we identified the sequence variant Val274Ile (Fig. 1*b*). This variant occurs at an absolutely conserved residue within the SMIR domain, is common in unaffected populations (3% in European-descended and 22% in Asian populations) and is an attractive candidate for a modifier of VWS, PPS, and other orofusial clefting disorders.

The mixed clefting phenotype is common in families affected with VWS, but very rare in families with non-syndromic orofacial clefts, and is not seen in most other syndromic forms of orofacial clefts. It is, however, also seen in clefting disorders caused by mutations in the genes *MSX1* (ref. 18) and *TP63* (ref. 19,20), suggesting that these may be involved in a common genetic pathway. In support of a common pathway, we found two IRF binding sites in the promoter of *MSX1* and one in the intron, all of which are conserved between human and mouse.

Table 1 • *IRF6* mutations

Family	Mutation	nt change	aa change	Exon
VWS1	frameshift	A–48T	5′UTR to Met	2
VWS2	frameshift	G3A	Met1Ile	3
VWS3	missense	C5T	Ala2Val	3
VWS4	frameshift	17ins(C)	Arg6fs	3
VWS35	frameshift	49del (CAGGTGGATAGTGGCC)	Gln17fs	3
VWS5	missense	G52A	Val18Met	3
VWS36	missense	T53C	Val18Ala	3
VWS37	nonsense	C69A	Tyr23X	3
VWS6	missense	C115G	Pro39Ala	3
PPS1	missense	T178G	Trp60Gly	4
VWS7	missense	C182G	Ala61Gly	4
PPS2	missense	A197C	Lys66Thr	4
VWS8	nonsense	C202T	Gln68X	4
VWS9	nonsense	C202T	Gln68X	4
VWS10	missense	G208C	Gly70Arg	4
VWS11	missense	G208C	Gly70Arg	4
VWS45	missense	C226T	Pro76Ser	4
PPS13	missense	C244A	Gln82Lys	4
PPS3	missense	C250T	Arg84Cys	4
PPS4	missense	C250T	Arg84Cys	4
PPS5	missense	C250T	Arg84Cys	4
PPS6	missense	C250T	Arg84Cys	4
PPS7	missense	C250T	Arg84Cys	4
PPS8	missense	G251A	Arg84His	4
PPS9	missense	G251A	Arg84His	4
VWS12	missense	A262C	Asn88His	4
PPS10	missense	A265G	Lys89Glu	4
VWS13	missense	A268G	Ser90Gly	4
VWS14	nonsense	G274T	Glu92X	4
VWS41	nonsense	G274T	Glu92X	4
VWS15	missense	G292C	Asp98His	4
VWS16	nonsense	C352T	Gln118X	4
VWS17	frameshift	466ins(C)	His156fs	5
VWS18	nonsense	C558A	Cys186X	6
VWS19	nonsense	G576A	Trp192X	6
VWS20	frameshift	634in(CCAC)	Ser212fs	6
VWS21	frameshift	657del (CTCTCTCCC)ins(TA)	Ser219fs	6
VWS42	frameshift	744del(CTGCC)	Gly248fs	7
VWS22	missense	G749A	Arg250Gln	7
VWS43	nonsense	T759A	Tyr253X	7
VWS44	frameshift	795del(C)	Leu265fs	7
VWS23	missense	A818G	Gln273Arg	7
VWS24	frameshift	842del(A)	His281fs	7
VWS25	deletion	870del (CACTAGCAAGCTGCTGGAC)ins(A)	FTSKLLD290L	7
VWS46	missense	T881C	Leu294Pro	7
VWS26	missense	G889A	Val297Ile	7
VWS38	missense	A958G	Lys320Glu	7
VWS39	missense	A958G	Lys320Glu	7
VWS27	missense	G961A	Val321Met	7
VWS40	missense	G974A	Gly325Glu	7
VWS28	missense	T1034C	Leu345Pro	7
VWS29	missense	G1040T	Cys347Phe	7
VWS30	missense	T1106C	Phe369Ser	8
VWS31	missense	C1122G	Cys374Trp	8
VWS32	missense	A1162G	Lys388Glu	8
PPS11	nonsense	C1177T	Gln393X	8
VWS33	nonsense	C1234T	Arg412X	9
PPS12	missense	G1288A	Asp430Asn	9
VWS34	frameshift	1381ins(C)	Pro461fs	9

Nucleotide position is relative to start codon. Mutations in the DNA-binding and SMIR/IAD domains are located in the top and bottom box, respectively.

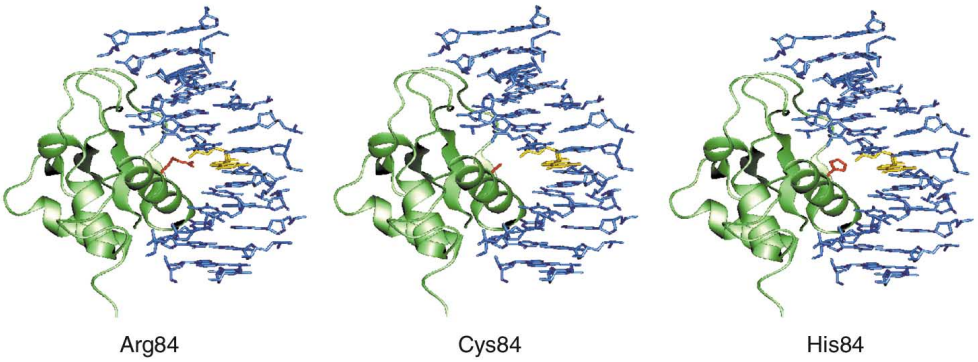

Fig. 2 Protein modeling of IRF6. The predicted IRF6 protein structure was aligned with the crystalline structure of the DNA-binding domain of IRF1. In the wildtype protein (green), the Arg84 residue (red) binds to the guanine (yellow) in the consensus sequence GAAA (blue), found in the IFN-β promoter, by means of three interactions. A bidentate hydrogen bond forms between two amine groups in the guanine base and the two amine groups in the basic side chain of the arginine, measuring a distance of 2.6 Å. An electrostatic 2.2-Å salt link also forms between the positively charged amine group of the arginine and the negatively charged 5′ phosphate group that precedes the guanine base. In the Arg84Cys mutant, the gap between the cysteine side chain and guanine base is greater than 3.10 Å, and is thus too great to support a hydrogen bond. Cysteine cannot physically form hydrogen or electrostatic bonds with the DNA, and this results in a disrupted DNA–protein interaction. In the Arg84His mutant, the aromatic ring of the histidine side chain is predicted to be oriented perpendicular to the DNA groove. This position would reduce the flexibility of the protein, impeding its ability to hydrogen bond.

We are taking an integrated approach to dissecting the complex pathways that underlie development of the lip and palate, including genetic analysis to identify the mutations that cause orofacial clefts. The discordant monozygotic twins proved useful in this effort, and provided proof of principle[21] that discordant monozygotic pairs can be used to search for modifiers or mutations, especially in regard to complex traits where mapping may be imprecise and mutation analysis may be confounded by SNPs. We also used a large number of samples from unrelated individuals to confirm that mutations in *IRF6* are pathogenic for both VWS and PPS and to prove that IRF6 is essential for development of the lip and palate and is involved in development of the skin and external genitalia. The SMIR domain has been proposed to mediate an interaction between IRFs and Smads[13], a family of transcription factors known to transduce TGF-β signals[22]. In addition, the expression of *Irf6* along the medial edge of the palate seems to overlap with *Tgfb3* (ref. 23), and *Tgfb3*, along with other members of this superfamily such as *Tgfb2* and *Inhba*, is required for palatal fusion[24–27]. Together with our data, these observations support a role for IRF6 in the transforming growth factor-β (TGF-β) signaling pathway, a developmental pathway of fundamental significance. The identification of IRF6 as a key determinant in orofacial development will help us to further delineate and integrate the molecular pathways underlying morphogenesis of the lip and palate.

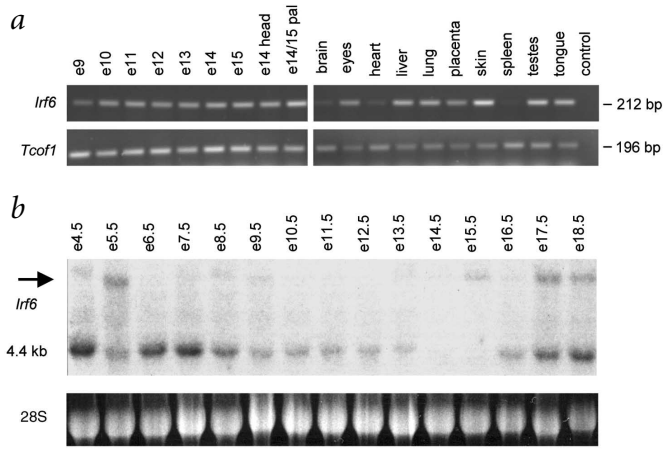

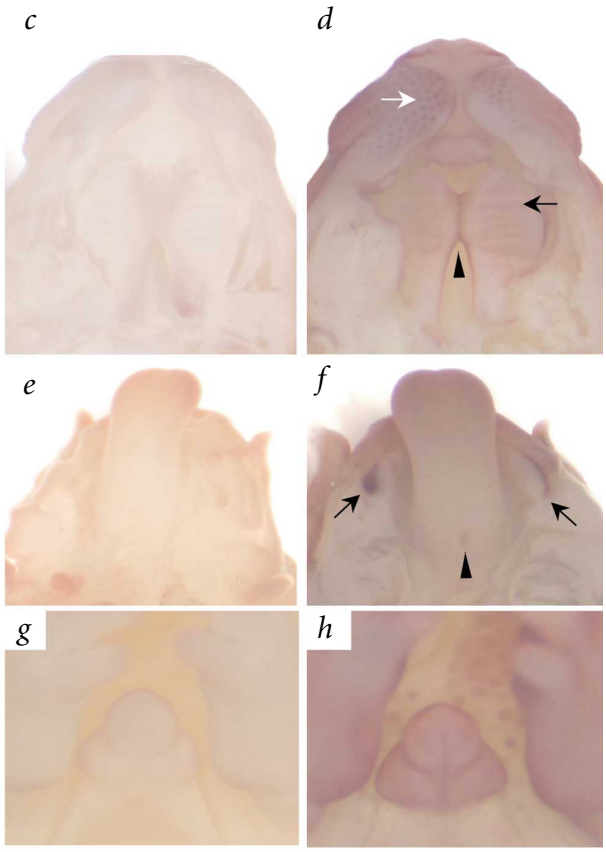

Fig. 3 Expression of mouse *Irf6*. ***a***, RT–PCR analysis of mouse tissues. *Irf6* is expressed throughout a range of embryonic and adult tissues, although at low levels in brain, heart and spleen. Greater *Irf6* expression seems to occur in secondary palates dissected from day 14.5–15 mouse embryos and in adult skin. PCR reactions carried out for 25 (not shown), 30 (shown) and 35 (not shown) cycles yielded similar results. Control RT–PCR experiments were done using the ubiquitously expressed gene *Tcof1* (ref. 28). ***b***, Northern-blot analysis of total RNA derived from whole mouse embryos at the day indicated. The *Irf6* probe detects a transcript of approximately 4 kb and a larger transcript (arrow) whose size could not be determined. The amount of total RNA loaded into each lane was verified by ethidium bromide staining of the 28S rRNA transcript. ***c–h***, Whole-mount *in situ* hybridization of day 14.5 mouse embryos. High *Irf6* expression is observed in the hair follicles (*d*, white arrow), palatal rugae (*d*, black arrow), medial edge of the secondary palate immediately before and during fusion (*d*, arrowhead), mandibular molar tooth germs (*f*, arrow), thyroglossal duct (*f*, arrowhead) and penis (*h*). *c*,*e*,*g*, Embryos from the same litter hybridized with the sense probe are presented for comparison.

Methods

Families. Families affected with VWS (n = 107) and PPS (n = 15) were identified and examined by one or more geneticists or clinicians as previously described[12]. Nearly all families are of northern European descent. Sample collection and inclusion criteria for VWS and PPS were described previously[3]. We obtained written informed consent from all subjects and approval for all protocols from the Institutional Review Boards at the University of Iowa and at the University of Manchester.

Mutation analysis. We amplified exons 1–8 and part of exons 9 and 10 by standard PCR. The primer sequences are available on request. The amplified products were purified (Qiagen) and directly sequenced with an ABI Prism 3700. The sequence was analyzed using the computer program PolyPhred.

Protein modeling. The IRF6 protein structure was predicted from its amino-acid sequence using Expasy, and aligned with the known crystalline structure of the DNA-binding domain of IRF1 using the UNIX-based computer software package Quanta (Accelrys). To model the mutations found at position Arg84 in the IRF6 DNA-binding domain, the residue was manually altered to a cysteine or a histidine. The package predicts all possible orientations of the altered side chain and displays the position with the highest probability.

RT–PCR. We extracted total RNA using a standard guanidinium isothiocyanate, acid–phenol protocol. RT–PCR analyses were performed and analyzed as detailed previously[28] using a forward primer designed in exon 4 and a reverse primer designed in exon 6 of *Irf6*. These primers generate a single product of 212 bp from cDNA.

Northern-blot analysis. A multiple-tissue northern blot (Seegene) was hybridized with a probe generated by PCR using primers derived from the distal end of the 3′ untranslated region of *Irf6* and labeled as recommended by the manufacturer with the StripE-Z system (Ambion). We hybridized the blot in Express Hyb (Clontech), washed it as recommended and exposed it to X-ray film for 72 h at –80 °C.

Whole-mount *in situ* hybridization. Sense and anti-sense riboprobes were 1,600 bp in length, derived from the 3′ untranslated region of *Irf6* and generated with Sp6 and T7 promoters, respectively. We fixed embryos dissected from time-mated MF1 mice in 4% paraformaldehyde overnight, processed them and subjected them to hybridization with sense or anti-sense probes as described previously[29].

Statistical analysis. Statistical significance of mutation location was calculated with the Fisher's exact test using the assumption of equal probability for a mutation at each residue.

URL. PolyPhred, http://droog.mbt.washington.edu/PolyPhred.html; Expasy, www.expasy.ch.

Acknowledgments

We thank our many clinical colleagues and their patients for contributing samples for this study (N. Akarsu, M. Aldred, Z. Ali-Khan, W.P. Allen, L. Bartoshesky, B. Bernhard, E. Bijlsma, E. Breslau-Siderius, C. Brewer, L. Brueton, B. Burton, J. Canady, A. Chakravarti, K. Chen, J. Clayton-Smith, M. Cunningham, A. David, B.B.A. de Vries, F.R. Desposito, K. Devriendt, R. Falk, J.-P. Fryns, R.J.M. Gardner, M. Golahi, J. Graham, M. Greenstein, M. Hannibal, E. Hauselman, R. Hennekam, G. Hoganson, L. Holmes, J. Hoogeboom, E. Hoyme, S. Kirkpatrick, J. Klein, T.C. Matise, L. Meisner, Z. Miedzybrodzka, J. Mulliken, A. Newlin, R. Pauli, W. Reardon, S. Roberts, H. Saal, A. Schinzel, J. Siegel-Bartelt, D. Sternen, V. Sybert, D. Tiziani, M.-P. Vazquez, L. Williamson-Kruse, F. Wilt, C. Yardin and K. Yoshiura). We appreciate the advice of K. Buetow, J. Dixon and C. Baldock; technical assistance from S. Hoper, M. Malik, J. Allaman, C. Hamm, N. Rorick, C. Nishimura, B. Ludwig, M. Fang, P. Hemerson, A. Westphalen and S. Lilly; administrative support from K. Krahn, D. Benton and L. Muilenburg; and sharing of unpublished results by P. Jezewski, A. Grossman and T.W. Mak. This work was supported by grants from the US National Institutes of Health and by grants to M.J.D. from Wellcome Trust, Action Research, Biotechnology and Biological Sciences Research Council, The European Union and the Fundação Lucentis (R.L.L.F.L. & D.M.F.).

Competing interests statement

The authors declare that they have no competing financial interests.

Received 23 May; accepted 5 August 2002.

1. Taniguchi, T., Ogasawara, K., Takaoka, A. & Tanaka, N. IRF family of transcription factors as regulators of host defense. *Annu. Rev. Immunol.* **19**, 623–655 (2001).
2. Murray, J.C. *et al*. Linkage of an autosomal dominant clefting syndrome (Van der Woude) to loci on chromosome 1q. *Am. J. Hum. Genet.* **46**, 486–491 (1990).
3. Schutte, B.C. *et al*. A preliminary gene map for the Van der Woude syndrome critical region derived from 900 kb of genomic sequence at 1q32-q41. *Genome Res.* **10**, 81–94 (2000).
4. Van der Woude, A. Fistula labii inferioris congenita and its association with cleft lip and palate. *Am. J. Hum. Genet.* **6**, 244–256 (1954).
5. Gorlin, R.J., Sedano, H.O. & Cervenka, J. Popliteal pterygium syndrome. A syndrome comprising cleft lip-palate, popliteal and intercrural pterygia, digital and genital anomalies. *Pediatrics* **41**, 503–509 (1968).
6. Bixler, D., Poland, C. & Nance, W.E. Phenotypic variation in the popliteal pterygium syndrome. *Clin. Genet.* **4**, 220–228 (1973).
7. Lees, M.M., Winter, R.M., Malcolm, S., Saal, H.M. & Chitty, L. Popliteal pterygium syndrome: a clinical study of three families and report of linkage to the Van der Woude syndrome locus on 1q32. *J. Med. Genet.* **36**, 888–892 (1999).
8. Sachidanandam, R. *et al*. A map of human genome sequence variation containing 1.42 million single nucleotide polymorphisms. *Nature* **409**, 928–933 (2001).
9. Fraser, F.C. Thoughts on the etiology of clefts of the palate and lip. *Acta Genetica* **5**, 358–369 (1955).
10. Bocian, M. & Walker, A.P. Lip pits and deletion 1q32–q41. *Am. J. Med. Genet.* **26**, 437–443 (1987).
11. Sander, A., Schmelzle, R. & Murray, J. Evidence for a microdeletion in 1q32–41 involving the gene responsible for Van der Woude syndrome. *Hum. Mol. Genet.* **3**, 575–578 (1994).
12. Schutte, B.C. *et al*. Microdeletions at chromosome bands 1q32-q41 as a cause of Van der Woude syndrome. *Am. J. Med. Genet.* **84**, 145–150 (1999).
13. Eroshkin, A. & Mushegian, A. Conserved transactivation domain shared by interferon regulatory factors and Smad morphogens. *J. Mol. Med.* **77**, 403–405 (1999).
14. Mamane, Y. *et al*. Interferon regulatory factors: the next generation. *Gene* **237**, 1–14 (1999).
15. Au, W.C., Yeow, W.S. & Pitha, P.M. Analysis of functional domains of interferon regulatory factor 7 and its association with IRF-3. *Virology* **280**, 273–282 (2001).
16. Escalante, C.R., Yie, J., Thanos, D. & Aggarwal, A.K. Structure of IRF-1 with bound DNA reveals determinants of interferon regulation. *Nature* **391**, 103–106 (1998).
17. Lin, R., Heylbroeck, C., Genin, P., Pitha, P.M. & Hiscott, J. Essential role of interferon regulatory factor 3 in direct activation of RANTES chemokine transcription. *Mol. Cell Biol.* **19**, 959–966 (1999).
18. van den Boogaard, M.J., Dorland, M., Beemer, F.A. & van Amstel, H.K. MSX1 mutation is associated with orofacial clefting and tooth agenesis in humans. *Nature Genet.* **24**, 342–343 (2000).
19. Celli, J. *et al*. Heterozygous germline mutations in the p53 homolog p63 are the cause of EEC syndrome. *Cell* **99**, 143–153 (1999).
20. McGrath, J.A. *et al*. Hay-Wells syndrome is caused by heterozygous missense mutations in the SAM domain of p63. *Hum. Mol. Genet.* **10**, 221–229 (2001).
21. Machin, G.A. Some causes of genotypic and phenotypic discordance in monozygotic twin pairs. *Am. J. Med. Genet.* **61**, 216–228 (1996).
22. Brivanlou, A.H. & Darnell, J.E., Jr. Signal transduction and the control of gene expression. *Science* **295**, 813–818 (2002).
23. Fitzpatrick, D.R., Denhez, F., Kondaiah, P. & Akhurst, R.J. Differential expression of TGF β isoforms in murine palatogenesis. *Development* **109**, 585–595 (1990).
24. Proetzel, G. *et al*. Transforming growth factor-β3 is required for secondary palate fusion. *Nature Genet.* **11**, 409–414 (1995).
25. Sanford, L.P. *et al*. TGFβ2 knockout mice have multiple developmental defects that are non-overlapping with other TGFβ knockout phenotypes. *Development* **124**, 2659–2670 (1997).
26. Matzuk, M.M. *et al*. Functional analysis of activins during mammalian development. *Nature* **374**, 354–356 (1995).
27. Kaartinen, V. *et al*. Abnormal lung development and cleft palate in mice lacking TGF-β 3 indicates defects of epithelial–mesenchymal interaction. *Nature Genet.* **11**, 415–421 (1995).
28. Dixon, J., Hovanes, K., Shiang, R. & Dixon, M.J. Sequence analysis, identification of evolutionary conserved motifs and expression analysis of murine tcof1 provide further evidence for a potential function for the gene and its human homologue, TCOF1. *Hum. Mol. Genet.* **6**, 727–737 (1997).
29. Nieto, M.A., Patel, K. & Wilkinson, D.G. *In situ* hybridization analysis of chick embryos in whole mount and tissue sections. *Methods Cell Biol.* **51**, 219–235 (1996).